

# Entanglement in low-energy states of the random-hopping model

Giovanni Ramírez,<sup>1,\*</sup> Javier Rodríguez-Laguna,<sup>2</sup> and Germán Sierra<sup>1</sup>

<sup>1</sup>*Instituto de Física Teórica, UAM-CSIC, Madrid, Spain*

<sup>2</sup>*Mathematics Dept., Universidad Carlos III de Madrid, Spain*

(Dated: Mar. 7, 2014)

We study the low-energy states of the 1D random-hopping model in the strong disordered regime. The entanglement structure is shown to depend solely on the probability distribution for the length of the effective bonds  $P(l_b)$ , whose scaling and finite-size behavior are established using renormalization-group arguments and a simple model based on random permutations. Parity oscillations are absent in the von Neumann entropy with periodic boundary conditions, but appear in the higher moments of the distribution, such as the variance. The particle-hole excited states leave the bond-structure and the entanglement untouched. Nonetheless, particle addition or removal deletes bonds and leads to an effective saturation of entanglement at an effective block size given by the expected value for the longest bond.

PACS numbers: 74.62.En, 71.23.-k, 03.67.Mn, 75.10.Pq

## I. INTRODUCTION

The interplay between disorder and entanglement in low-dimensional systems has proved to be a rich source of problems and surprises. Anderson's theorem [1] states that, in one-dimensional systems with uncorrelated disorder in the local potential, all single-body states will localize and, thus, real space blocks within the ground state present nearly no entanglement. Entanglement entropy is, nonetheless, a good indicator of the localization-delocalization quantum phase transition in higher dimensions [2]. On the other hand, off-diagonal disorder, as it appears in the random variants of the XX or Ising models, leads in certain cases to long-range correlations and logarithmic violations of the area law.

Let us focus on a relevant special case in which the clean system is in a 1D critical state, described by a certain conformal field theory (CFT) with central charge  $c$ . The von Neumann entropy of a block of  $\ell$  contiguous sites in a system of size  $L$  with periodic boundary conditions follows the law [3–5]

$$S(\ell) \approx \frac{c}{3} \log(\ell). \quad (1)$$

There is ample evidence that the inclusion of strong off-diagonal disorder between nearest neighbors gives raise to a disorder-averaged von Neumann entropy similar to eq. (1), but with a different *effective* value for the central charge [6]:

$$\langle S(\ell) \rangle \approx \frac{c \log(s)}{3} \log(\ell) + c', \quad (2)$$

where  $\log(s)$  is the von Neumann entropy of the ground state of a system with two sites. Indeed, the striking similarities between the clean and the strongly disordered

systems are even deeper than expression (2) suggests, since they also appear in the averages for the correlation functions and the finite-size effects in entanglement [7]. Those similarities will be the main focus of this work.

In this work we will consider the random-XX model or, in other terms, the fermionic random-hopping Hamiltonian in 1D:

$$\mathcal{H} = - \sum_i J_i c_i^\dagger c_{i+1} + \text{h.c.} \quad (3)$$

In the clean case, the system is critical, and the central charge of the associated CFT is  $c = 1$ . The  $\log(s)$  factor is found by considering what is the entanglement entropy between sites in a  $L = 2$  system, i.e.:  $\log(s) = \log(2)$ . Thus, we can fill in the values  $c = 1$  and  $s = 2$  in expression (2).

Whenever the  $J_i$  are different, expression (3) is called the *inhomogeneous hopping* model, which is exactly solvable: diagonalizing the hopping matrix one can study the single particle energy levels  $\epsilon_k$  and the single particle modes  $v_{k,i}$ , where  $k$  denotes the eigenvalue number and  $i$  the actual site. When the different *hoppings*  $J_i$  vary slowly with position, they can be regarded as a modulation on the speed of sound. Indeed, a careful choice for the  $J_i$  can be used to model quantum matter on a curved space-time background [8]. The modes have some generic mathematical properties, such as particle-hole symmetry: a canonical transformation  $c_i^\dagger \rightarrow (-1)^i c_i^\dagger$  transforms  $\mathcal{H} \rightarrow -\mathcal{H}$ . Thus, if  $\{v_{k,i}\}_{i=1}^L$  is a mode with energy  $\epsilon_k$ , then  $\{(-1)^i v_{k,i}\}_{i=1}^L$  is also a mode with energy  $-\epsilon_k$ . In absence of zero modes, the ground state can be proved to take place at half filling and is spatially homogeneous.

Let us consider the  $\{J_i\}$  to be independent random variables extracted from a probability distribution  $p_\delta(J)$  pertaining to the following family

$$p_\delta(J) \equiv \frac{1}{\delta} J^{-1+\frac{1}{\delta}} \quad (4)$$

for  $0 < J < 1$  and  $\delta > 0$ ;  $\delta$  characterizes the randomness, i.e.  $\delta = 1$  for the uniform distribution. We will focus on

\*Electronic address: giovanni.ramirez@uam.es

the  $\delta \rightarrow \infty$  limit, the so-called strong disorder regime [6], in which the sampled  $J$  span many orders of magnitude in the interval  $(0,1)$ . In this regime, the renormalization group (RG) derived by Dasgupta and Ma [9] gives an accurate description of the ground state. It proceeds through decimation: at each RG step, we select the highest hopping and put a fermion resonating between the two sites, i.e.: a *bond*. In the spin-chain view, we would speak of a singlet between both spins. The two sites are then removed from the chain, and their neighbors are linked by a new effective hopping term. The procedure is repeated and, when it is finished, the ground state can be written as a *random bond* (or random singlet) structure. Under successive applications of the Dasgupta-Ma RG approach, the probability distribution for the remaining hoppings,  $p_\delta(J)$  flows by increasing the value of  $\delta$ , and  $\delta \rightarrow \infty$  is the (unattainable) infinite-randomness fixed point (IRFP) [10, 11]. That is the reason for our choice to focus on the strong disorder limit.

The aim of this work is to illuminate the surprising relation between entanglement in critical states, as described by CFT, and average entanglement entropies in strongly disordered systems. In section II we will discuss the techniques which will be employed to obtain expectation values of entanglement measures, using both exact diagonalization and the RG. In section III we will discuss the finite-size scaling of the average von Neumann and Rényi block entropies within the ground state of our model. The statistics of the bond lengths is discussed in detail in section IV. By successive distillation of the basic physics we will reach a simple model which yields accurate predictions for average entropies, based solely on the analysis of random permutations in section V. The study of the excited states, performed in section VI, benefits from the different approaches discussed before. Section VII is devoted to the exposition of conclusions and further work.

## II. COMPUTING ENTANGLEMENT ENTROPIES

Our aim is to study the statistical properties of the entanglement of the ground state of Hamiltonian (3) on a 1D system with size  $L$  and periodic boundary conditions (PBC), when the couplings  $\{J_i\}$  are chosen as independent random variables from the probability distribution (4), specially in the strong disorder limit  $\delta \rightarrow \infty$ . The physics of the low-energy eigenstates of Hamiltonian (3) can be analyzed with two methods:

1.- *Exact Diagonalization (ED)*. In order to obtain the ground state of (3) it suffices to diagonalize the hopping matrix  $T_{ij}$ , with  $i, j \in \{1, \dots, L\}$ , whose non-zero elements are  $T_{i,i+1} = T_{i+1,i} = -J_i$ . Its eigenstates,  $Tv_k = \epsilon_k v_k$ , constitute the modes, which allow us to

compute the correlation matrix:

$$C_{ij} \equiv \langle c_i^\dagger c_j \rangle = \sum_{k=1}^{N_e} \bar{v}_{k,i} v_{k,j}, \quad (5)$$

for the ground state of the system: a Fermi state of  $N_e$  fermions. Given any block  $B$  of  $\ell$  sites in the system, the eigenvalues of the reduced density matrix, i.e.: its entanglement spectrum, can be obtained using a reverse form of Wick's theorem [12]. Let  $\nu_k$  be the eigenvalues of the correlation matrix when restricted to that block, then the reduced density matrix  $\rho^B$  of the block is a product of density matrices of single-site blocks  $\bigotimes_k^\ell \rho_k$  and the  $\alpha$ -th order Rényi entropy can be obtained as a sum of the entropies of  $\rho_k = \nu_k d_k^\dagger d_k + (1 - \nu_k) d_k d_k^\dagger$  where  $d$  and  $d^\dagger$  are other fermionic operators

$$S_\alpha(B) = \frac{1}{1-\alpha} \sum_k [\nu_k^\alpha + (1 - \nu_k)^\alpha] \quad (6)$$

and the von Neumann entropy for the block corresponds to the limit  $\alpha \rightarrow 1$ ,

$$S_1(B) = - \sum_k [\nu_k \log(\nu_k) + (1 - \nu_k) \log(1 - \nu_k)]. \quad (7)$$

The application of this technique in our case presents a serious problem: the diagonalization of the hopping matrix is a highly ill-conditioned problem, since their eigenvalues differ by many orders of magnitude. Thus, it is a numerical challenge to obtain the actual block entropy, given a realization of the  $\{J_i\}$ . In practice, it is unfeasible to study systems with either  $L$  or  $\delta$  too large.

2.- *Dasgupta-Ma Renormalization Group (RG)*. Within the strong disorder regime, we can rely on the renormalization group (RG) scheme devised by Dasgupta and Ma [9] to find out the bond structure which describes the ground state of the system. This is a decimation procedure in which one chooses the strongest link,  $\max\{J_i\}$  and establishes a single-particle state as a bond on top of it. Then, the two neighboring sites are joined by a renormalized (effective) link, whose strength can be found using second-order perturbation theory:

$$J_k^{(R)} = \frac{J_{k-1} J_{k+1}}{J_k}. \quad (8)$$

The strongest link and its two neighbours are replaced by this (weaker) renormalized link, then we proceed to pick the second strongest link, and iterate the process until all the links have been renormalized (assuming even  $L$ ). At some moment, the strongest link will be one of the renormalized links in previous iterations. Thus, a long-distance bond will be established between two sites which were not nearest neighbors. Why do such long-distance bonds exist? The physical picture is illustrated in figure 1. Let us consider the particle at the rightmost site. It has a certain probability of hopping to its left, whenever the inner bond particle is also at its left site.

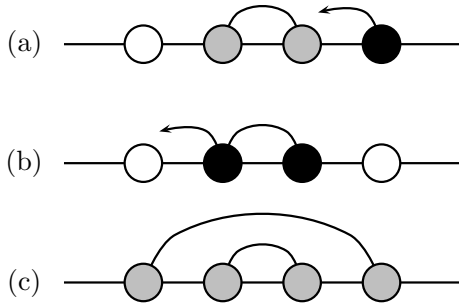


Figure 1: Illustration of the physical picture which induces long-distance bonds. (a) A bond has been established on the central link, which is very strong. A particle at the right extreme attempts to jump in. (b) Sometimes, the particle succeeds, and the central bond becomes doubly occupied. The left particle must jump out. (c) We can view the full procedure as a tunneling event through the occupied bond, with a much lower associated probability amplitude.

At this moment, the inner bond becomes doubly occupied. The original particle inside the inner bond is not allowed to hop rightwards, but it may hop leftwards. As particles are indistinguishable, the total procedure can be described as a tunneling of one particle through an established bond. The associated probability amplitude of this event is much lower than the probability amplitude of hopping in the inner bond, thus accounting for the large differences in energy between them. This procedure, which is akin to the Anderson mechanism describing the interaction between a magnetic impurity and the spin of a conduction electron, can be assigned an effective hopping amplitude using second-order perturbation theory, thus obtaining expression (8). Similarly, one can think of the second-order procedure which allows to find an effective Heisenberg Hamiltonian with  $J \approx t^2/U$  from a Hubbard system in the limit  $U \gg t$ .

When the decimation procedure is finished, we obtain a bond-structure, as those illustrated in figure (2), with many bonds of length one, but still with a large fraction covering larger distances. Notice that the random-bond state factorizes into pairs, i.e.: there is a pairing of the sites  $\{(i_1, j_1), (i_2, j_2), \dots, (i_{L/2}, j_{L/2})\}$ , such that the ground state for the system factorizes into the product of a singlet state for every pair. In other words, each pair  $(i_k, j_k)$  is disentangled from the rest of the system. The entanglement entropy of any block  $B$  can be found by simply counting the number of bonds which connect  $B$  to the rest of the system, and multiplying by  $\log(2)$ , which is the entropy associated to a single bond. Thus, the RG opens the possibility of a purely combinatorial solution to this problem, which will be discussed in section V. Notice that, within the bond picture, all Rényi entropies are equal.

Remarkably, the Dasgupta-Ma RG has recently received an interpretation within the tensor-networks and holography language [13].

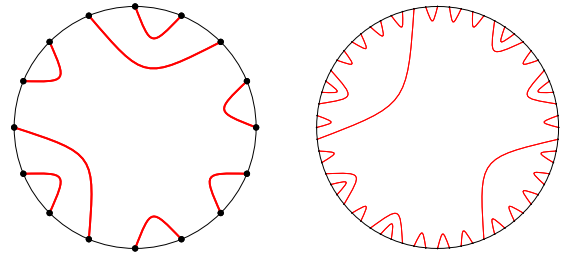


Figure 2: Example of bond structures, with 16 (left) and 64 sites (right) with periodic boundary conditions and  $\delta = 8$ .

### III. AVERAGE ENTANGLEMENT ENTROPIES IN THE GROUND STATE

Let  $S_\alpha(\ell)$  be the disorder-averaged Rényi entropy of a block of size  $\ell$  of order  $\alpha$ . When  $\alpha = 1$ , i.e., the von Neumann entropy, we will sometimes drop the index. Figure 3 compares the averaged Rényi entropies with both methods, exact diagonalization and RG, for a chain with PBC,  $L = 20$  and  $\delta = 10$ . The RG approach yields the same curve for all orders  $S_\alpha$ , while they differ for exact diagonalization. Notice that the RG entropy is closest to the  $S_1$  exact diagonalization entropy.

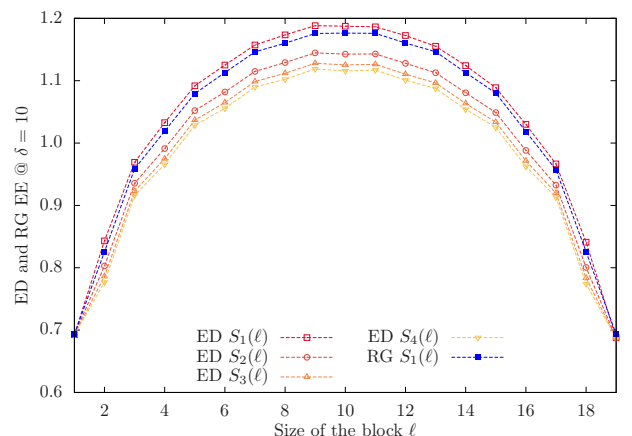


Figure 3: Average von Neumann and Rényi block entropies for a  $L = 20$  system with  $\delta = 10$ , comparing exact diagonalization and RG results for  $10^6$  realizations. Notice that the RG gives the same curve for all Rényi orders, which is closest to the von Neumann entropy obtained by exact diagonalization.

The difference between the RG predictions and the exact diagonalization results can be ascribed to inaccuracies in the bond-structure picture. Figure (4) shows a histogram of the values of the von Neumann entropy at half-chain for different disorder realizations. Notice that, as  $\delta$  increases, the behavior becomes closer to the bond-structure picture, which predicts a set of delta peaks at integer multiples of  $\log(2)$  [14].

The average half-chain von Neumann entropy

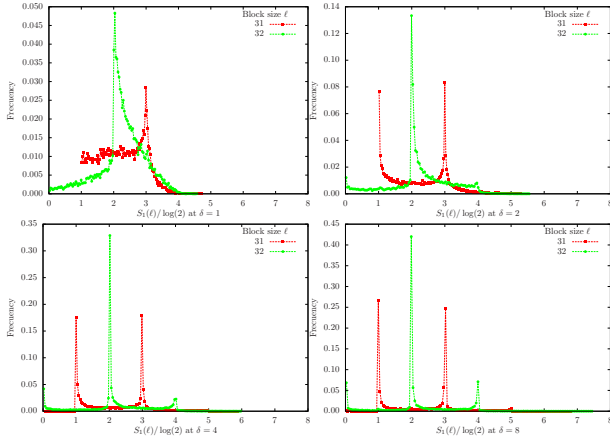


Figure 4: Histogram for the von Neumann entropy for odd-size blocks (red) and even-size blocks (green) for different values of  $\delta$  and  $L = 64$  for  $2 \cdot 10^4$  samples.

$\langle S_1(L/2) \rangle$  is specially useful to determine the global behavior disregarding finite-size effects. We have run five million realizations of the disorder with  $\delta = 10$  and  $L$  in the range from 64 to 2176, and obtained the average half-chain entropy as a function of  $L$  using the Dasgupta-Ma RG, as shown in the top panel of fig. 5. The fit to a form like (2) is very accurate [14, 15]:  $\langle S_1(L/2) \rangle$  grows logarithmically with a factor  $c \log(2)/3$ , and the fit for  $c \approx 1.015$ , i.e.: very close to 1. The additive constant is  $c' \approx 0.7639$ .

The average entropy for blocks of different sizes is shown in figure (5, bottom). We depict  $\langle S_1(\ell) \rangle - \langle S_1(L/2) \rangle$  as a function of the fraction of the chain occupied by the block,  $\ell/L$  using the same data. All the points collapse to a single scaling function, which we fit to a CFT finite-size form [16]

$$\tilde{S}(\ell) = S(\ell) - S(L/2) \approx \frac{c \log(2)}{3} \log \left[ \sin \left( \pi \frac{\ell}{L} \right) \right], \quad (9)$$

and plot the resulting curve along with the points. The difference between the fitting curve and the points is apparent, so we proceed to subtract them and plot the result in the inset of figure (5, bottom). The residual appears to correspond to *higher harmonics*, showing that a different scaling function,  $Y(x)$ , is required to account for the finite-size effects [7]. The Fourier series representation of that function can be written as

$$Y(x) = \left[ 1 + \sum_{j=1}^{\infty} k_j \right] \sin x - \sum_{j=1}^{\infty} \frac{k_j}{2j+1} \sin [(2j+1)x] \quad (10)$$

and the more general expression for the finite-size average von Neumann entropy is given by

$$S(\ell) \approx \frac{c \log(2)}{3} \log \left[ \frac{L}{\pi} Y \left( \pi \frac{\ell}{L} \right) \right] + c' \quad (11)$$

the contribution of the first modes provides a good approximation to the entropy. Fitting the finite-size data

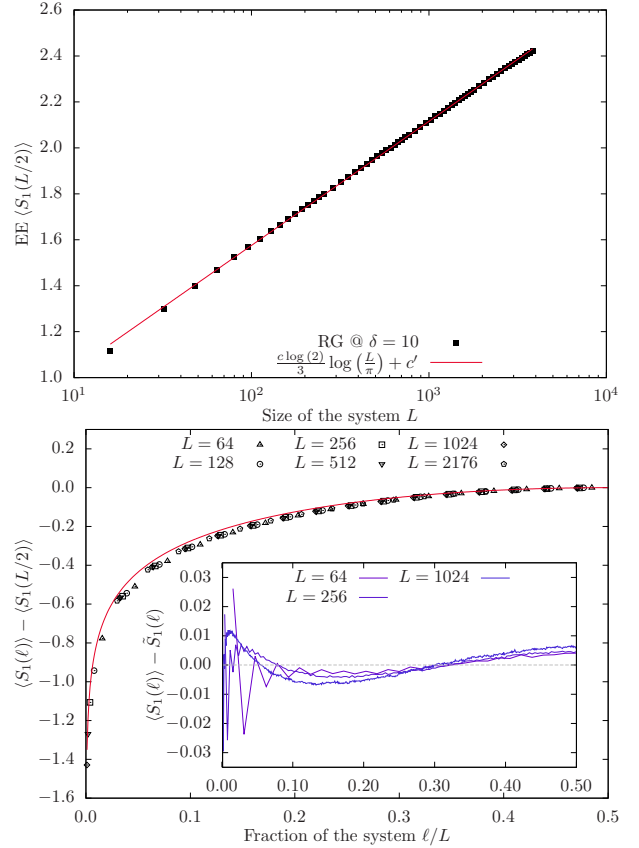


Figure 5: Top: average von Neumann entropy at half-chain  $\langle S_1(L/2) \rangle$  showing the characteristic logarithmic scaling with prefactor close to  $\log(2)/3$ . Bottom: vertically shifted data  $\langle S_1(\ell) \rangle - \langle S_1(L/2) \rangle$  for different system sizes  $L$  collapse into the continuous line, fitting  $\tilde{S}(\ell)$ . Inset: residual error when the fitted expression is compared with the data, note the presence of higher harmonics.

to this new functional form, we find the additive constant  $c' \approx 0.7338$  and the amplitude of the first mode  $k_1 = 0.1025$ , which are close to the value  $c' \approx 0.726$  reported by Laflorencie and [14] and the value  $k_1 = 0.115$  obtained by Fagotti et al. [7].

Despite the many similarities between the average behavior of entanglement in the random hopping model and a conformally invariant system in 1D, there are also substantial differences. One of the most relevant is in the Rényi entropies. In the conformal case they present characteristic parity oscillations [5, 17]:

$$S_\alpha(\ell) \approx \frac{c}{6} \left( 1 + \frac{1}{\alpha} \right) \log \left[ \frac{L}{\pi} \sin \left( \pi \frac{\ell}{L} \right) \right] + c' + (-1)^\ell f_\alpha \left[ \frac{L}{\pi} \sin \left( \pi \frac{\ell}{L} \right) \right]^{-2K/\alpha} \quad (12)$$

where  $c$  and  $c'$  are the same as in eq. (9),  $f_\alpha$  is the oscillation amplitude, which typically increases with  $\alpha$ ,  $K$  is the Luttinger parameter ( $K = 1$  in our case) and the term  $(-1)^\ell$  corresponds to  $\cos(2k_F \ell)$ , where  $k_F = \pi/2$  is the

Fermi moment for half-filling. On the other hand, within the bond-structure picture, all Rényi entropies are equal to the von Neumann case since, in the strong disorder regime, an  $\ell$ -size block has  $2^\ell$ -fold degenerate eigenvalues  $2^{-\ell}$  [6] then, the  $\alpha$  order Rényi entropy is

$$S_\alpha = \frac{1}{1-\alpha} \log 2^{\ell(1-\alpha)} = \log 2^\ell \quad (13)$$

Figure (6) compares the average Rényi entropies obtained with exact diagonalization in the clean and strongly disordered cases for a system with  $L = 64$ ,  $\delta = 8.5$  using  $2 \cdot 10^4$  disorder realizations, for the lowest Rényi orders ( $\alpha$  from 1 to 4). The upper panel shows the clean case, notice the strong parity oscillations in the higher order Rényi entropies. The bottom panel depicts the average Rényi entropies in the disordered case. Notice that their amplitude is substantially lower. The inset in the lower panel of figure (6) analyses that decrease in amplitude: the  $f_\alpha$  factors fitted in eq. (12) are plotted against  $\delta$ , the disorder intensity. They can be seen to attenuate very slowly. In fact, even for very large  $\delta$  they are still not negligible showing that the conjecture in [18] holds. Nonetheless, for infinite disorder, the effect of  $f_\alpha$  will disappear.

#### A. Variance of the von Neumann entropy

The variance of the von Neumann entropy presents also interesting universal behavior alike to the CFT predictions, but with an interesting difference: parity oscillations remain even in the strong disorder regime, as the RG calculations show. Fig. (7) depicts the results of simulations run with  $10^6$  samples for sizes  $L = 32, 64, 128, 256, 512$  and  $1024$ , obtained with the RG and  $\delta = 8$ , along with a very accurate fit to a law similar to (12):

$$\begin{aligned} \sigma_S^2 = & c_\sigma \log(2) \log \left[ \frac{L}{\pi} \sin \left( \pi \frac{\ell}{L} \right) \right] + c'_\sigma \\ & + (-1)^\ell f_\sigma \left[ \frac{L}{\pi} \sin \left( \pi \frac{\ell}{L} \right) \right]^{-2K_\sigma} \end{aligned} \quad (14)$$

with  $c_\sigma \approx 0.4$ ,  $c'_\sigma \approx 0.46$ ,  $f_\sigma \approx 0.78$  and  $K_\sigma \approx 2/3$ . Remarkably, the oscillations are also present in the higher order cumulants of the distribution. They are only absent in the average.

The origin of those oscillations in the variance of the von Neumann entropy, and their accurate fit to the CFT expression is an open problem. These oscillations bear resemblance to the density oscillations found by [19] in a clean system, which are explained as an effect of the boundaries and subleading corrections to the CFT prediction.

Notice that the variance is always higher for the even blocks, and the even-odd difference is much larger for smaller blocks. Also let us remark that although the average number of outgoing bonds increases smoothly as

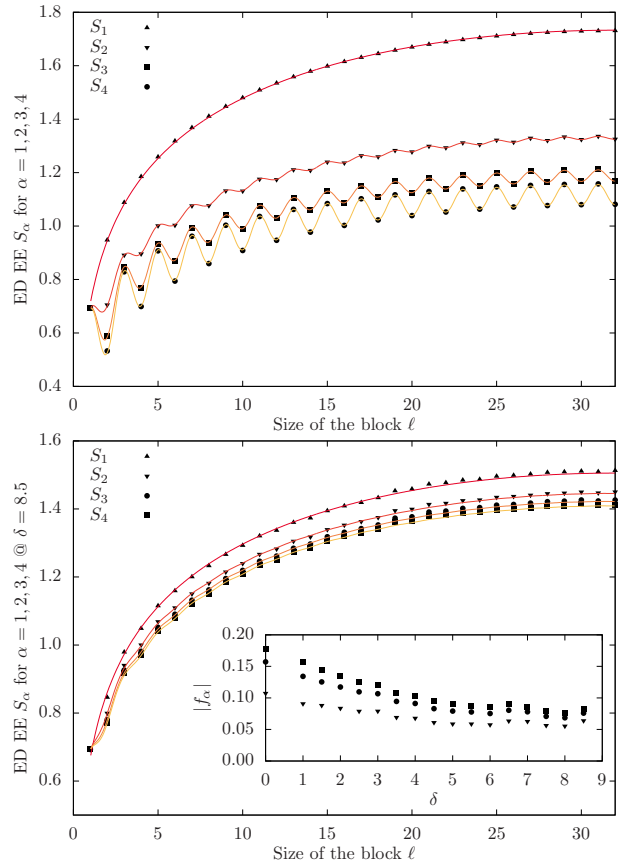


Figure 6: Top: Rényi block entropies in the clean case, for  $L = 64$  and PBC. Notice the strong parity oscillations in the higher order entropies. Bottom: average Rényi entropies for  $2 \cdot 10^4$  realizations of a  $L = 64$  system with  $\delta = 8.5$ . Notice how entropies of all orders become much closer, and how the oscillations attenuate. The inset shows a decrease in the magnitude of the oscillation amplitude  $f_\alpha$  in eq. (12) as a function of  $\delta$ .

we increase the block size, the probability distributions are quite different: even-sized blocks can only cut an even-number of bonds, and viceversa.

#### B. Open boundary conditions

Let us consider what are the differences in the case of open boundary conditions. In that case, translational invariance is lost: the entropy of a block depends not only on its size, but also on its distance to the extreme of the chain. It is customary to choose blocks starting from the left extreme. In that case block only presents one inner boundary instead of two. The CFT prediction for the clean (critical) case is that the prefactor of the logarithmic term in the expression of the von Neumann entropy is halved. In the disordered case we can also observe a reduction of the entanglement entropy, but with remarkable differences. Figure (8) shows the average von Neumann entropy for three sizes ( $L = 32, 64$  and

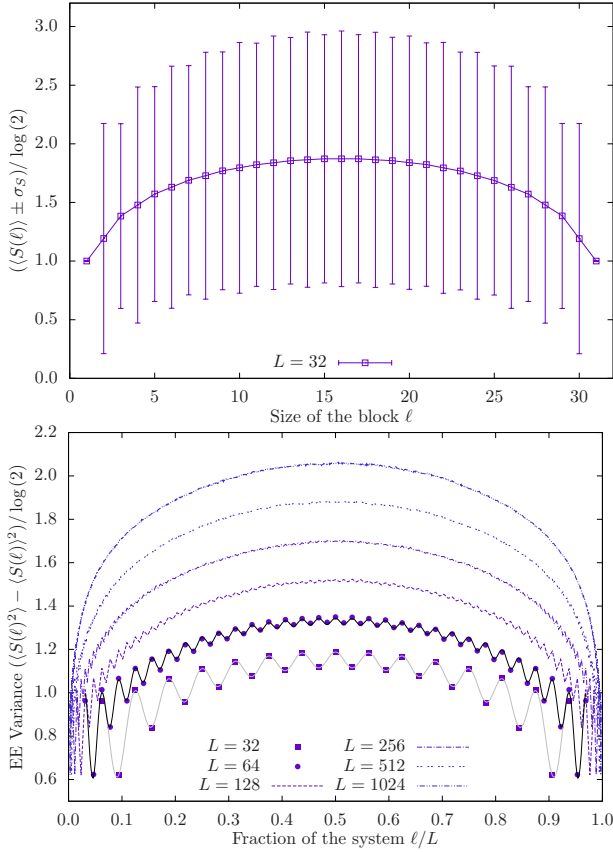


Figure 7: Top: average von Neumann entropy for  $\delta = 8$  and  $L = 32$ , obtained with the RG, with errorbars given by the standard deviation. Notice the parity oscillation in the errorbars, which are larger for even blocks. Bottom: variance of the von Neumann entropy distribution for different sizes and  $\delta = 8$ , obtained with the RG. Notice how the parity oscillations fit accurately expression (14).

128) with open boundary conditions, using  $10^6$  realizations with  $\delta = 8$ . Notice the parity oscillations, which are similar to those appearing in the higher order Rényi entropies with periodic boundary conditions. In fact, a fit to a expression similar to (12) works very well [20]

$$S(\ell) \approx \frac{c_{open} \log(2)}{6} \log \left[ \frac{L}{\pi} \sin \left( \pi \frac{\ell}{L} \right) \right] + c'_{open} + (-1)^\ell f_{open} \left[ \frac{L}{\pi} \sin \left( \pi \frac{\ell}{L} \right) \right]^{-K_{open}} \quad (15)$$

where  $c_{open} \approx 1.5$ ,  $c'_{open} \approx 0.76$ ,  $f_{open} \approx -0.24$  and  $K_{open} \approx 1$ . Thus, even though the entropy is reduced in the case of open boundary conditions, the results in this case differ considerably from the expectation that  $c_{open}$  should be one, but the value for  $K_{open}$  agrees with previous results obtained for clean systems [18, 21].

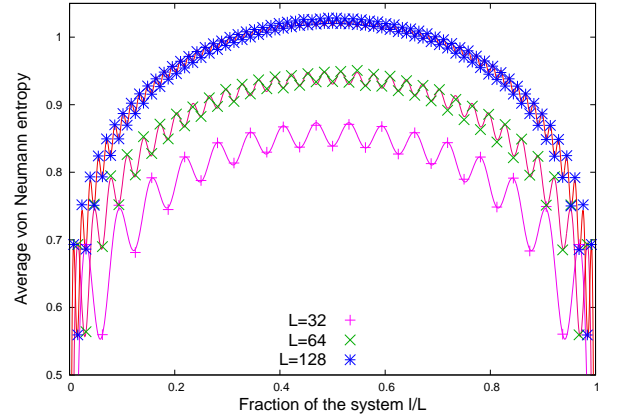


Figure 8: Average von Neumann entropy of the random hopping model with open boundary conditions. Notice the characteristic parity oscillations, which fit to a Luttinger parameter  $K = 1/2$ .

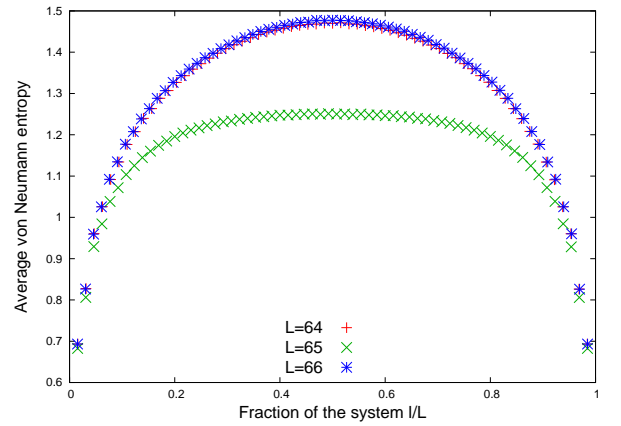


Figure 9: Average von Neumann entropy compared for even and odd number of sites. Notice the *plateau* which gets established for intermediate block sizes in the case of odd chains.

### C. Odd chains

On the other hand, disordered chains present very different behavior when the number of sites is *odd*, as opposed to the clean case. Effectively, in that case one site is not allowed to establish a bond, and entanglement is effectively reduced, see fig. (9). Moreover, bonds can not be established over the single site and, thus, this site can be regarded as an *opening* in the boundary conditions. Effectively, the average von Neumann entropy becomes nearly flat for intermediate block sizes, showing a *plateau*.

## IV. THE BOND-LENGTH DISTRIBUTION

Let us consider a 1D random hopping chain of length  $L$  and PBC, close enough to the IRFP, where the bond-structure picture becomes accurate to describe the ground state of the system. Given a bond between sites



$i_1$  and  $i_2$ , let  $l_b \equiv |i_1 - i_2| \pmod{L}$  be its length. Let us consider the probability distribution for the bond lengths,  $P(l_b)$ . As indicated in [22], we will show that all entanglement properties in the IRFP stem from the knowledge of this  $P(l_b)$  and the assumption of (approximate) bond independence, beyond the constraint that two bonds can never cut.

The scaling behavior of  $P(l_b)$  has been estimated via the Dasgupta-Ma RG [23]. As the RG proceeds, the typical length scale of the bonds increases. It can be argued that the likelihood of a given site surviving until the typical length scale is  $l_b$  scales as  $l_b^{-1}$ . A bond can be established only between two surviving sites, so, if we assume independence, the probability of establishing a bond of length  $l_b$  scales as the product:  $P(l_b) \approx l_b^{-2}$ . If that probability distribution is assumed to be exact for all (odd) values of  $l_b$ , the normalization constant should be  $8/\pi^2$ . But for small values of  $l_b$  the fitting exponent deviates from  $-2$ . For the scaling regime, the best fit is found to be  $P(l_b) \approx (2/3) l_b^{-2}$  [22].

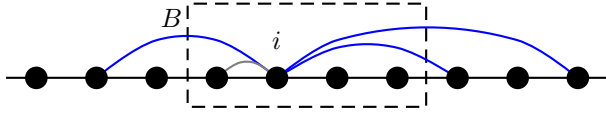


Figure 10: Illustration of the bond counting procedure which leads to expression (16). Let us consider box  $B$  of size  $\ell$ . Bonds stemming from site number  $i$  will contribute to the block entanglement only if their length is larger than their distance to the boundary (blue bonds only). Notice that actual bonds are only allowed if their length is *odd*.

The average von Neumann entropy of a block  $B$  with size  $\ell$  is given by the expected number of bonds crossing its boundaries, multiplied by  $\log(2)$ , see fig. (10). Let the sites in the block be numbered from 1 to  $\ell$ , and consider site  $i$  and its bond. Let  $i'$  be the other extreme. The bond will contribute to the entropy if its length is larger than the distance to the boundary. If  $i'$  is at the left of  $i$ , then the bond only contributes if  $l_b \geq i$ . The expected number of such bonds is  $\sum_{l_b=i}^{L/2} P(l_b)$ . If  $i'$  is at the right of  $i$ , the bond will contribute if  $l_b \geq \ell - i + 1$ , and we get  $\sum_{l_b=\ell-i+1}^{L/2} P(l_b)$ . Summing for all  $i$ , and considering that leftwards and rightwards bonds are equally likely, we get:

$$S_1(\ell) = \frac{\log(2)}{2} \sum_{i=1}^{\ell} \left[ \sum_{l_b=i}^{L/2} P(l_b) + \sum_{l_b=\ell-i+1}^{L/2} P(l_b) \right]. \quad (16)$$

This expression can be recollected into a more convenient one [22]:

$$S(\ell) = \log(2) \left[ \sum_{l_b=1}^{\ell} l_b P(l_b) + \ell \sum_{l_b=\ell+1}^{L/2} P(l_b) \right] \quad (17)$$

where the first term is the most relevant, since smaller bonds have the largest probabilities. Inserting the previous estimate for  $P(l_b) \approx (2/3) l_b^{-2}$  into the first term

of eq. (17), we obtain  $S(\ell) \approx (\log(2)/3) \log(\ell)$ , as in eq. (2).

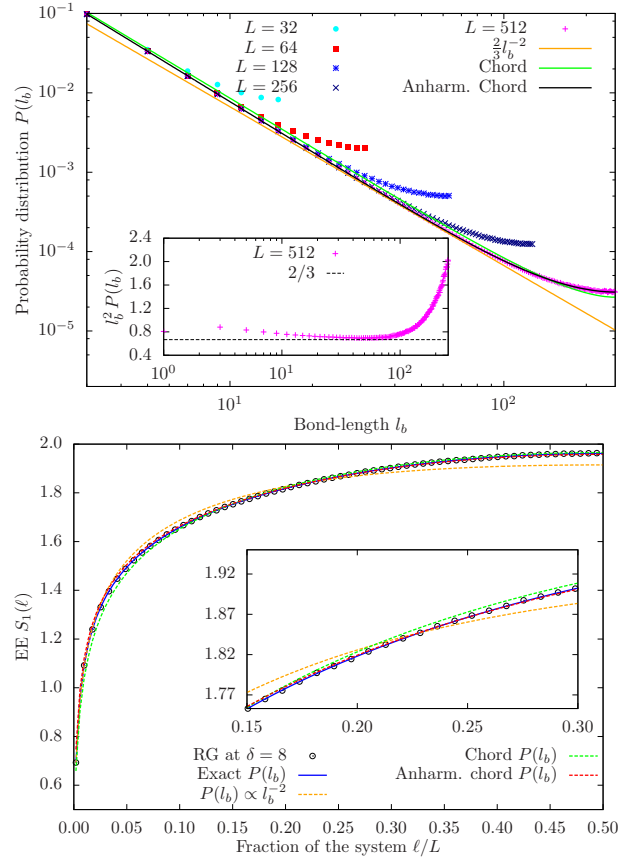


Figure 11: Top: Probability distribution for the bond-lengths obtained with the RG and  $\delta = 8$  for different sizes. Alongside, the scaling fit to intermediate bond-lengths,  $(2/3) l_b^{-2}$ , and the fits to the chord –eq. (18)– and the anharmonic chord –eq. (19). Inset: plot of  $l_b^2 P(l_b)$ , showing the approach to  $2/3$  during the scaling regime. Bottom: average von Neumann entropy for  $L = 512$  and  $\delta = 8$  (dots), along with predictions obtained by inserting different approximations to  $P(l_b)$  in eq. (17): the scaling law  $P(l_b) \propto l_b^{-2}$ , the chord approximations, and the exact  $P(l_b)$  obtained from the simulations. Notice that the accurate fit for this last one, validating expression (17). Inset: detail of the same plot.

Figure (11, top) studies the behavior of  $P(l_b)$  by averaging over five million disorder realizations with  $L$  ranging from 32 to 512 and  $\delta = 10$ , in logarithmic scale. The leading  $l_b^{-2}$  behavior is apparent, as a fit for intermediate values of  $l_b$  shows. The straight line corresponds to the scaling regime approximation,  $P(l_b) = (2/3) l_b^{-2}$ . The large- $l_b$  deviation, for  $l_b$  comparable to the system size, is a finite-size correction. Let us distribute the  $L$  points uniformly in a circumference of diameter 1. The probability for a bond between sites separated  $l_b$  lattice units is approximately proportional to the inverse squared of their actual distance, i.e., to their *chord*:

$$P(l_b) \propto \sin^{-2}(\pi l_b/L). \quad (18)$$

The accuracy of the fit to  $P(l_b)$  can be further improved using an *anharmonic* chord approximation:

$$P(l_b) \propto [Y(l_b)]^{-\gamma} \quad (19)$$

with  $Y(l_b)$  given in expression (10), and only retaining the first anharmonic term. The fit gives  $k_1 = 0.12$  and  $\gamma = 2.11$ , with very good accuracy.

Figure (11, bottom) compares the average entropy  $S(\ell)$  obtained by direct sampling with three possible estimates from the probability distribution for the bond-lengths using eq. (17): (i) the scaling law  $P(l_b) \propto l_b^{-2}$ , (ii) the chord and anharmonic-chord laws, eqs. (18) and (19), and (iii) the sampled distribution for  $P(l_b)$ . Notice that approximation (iii) is indistinguishable from the sampled entropy.

It is interesting to ask whether the bond-length samples are actually independent or not. We have investigated the bond-length correlations. Given a bond-structure, consider the list of the bond-lengths obtained when the bonds are ordered according to the index of their left-most site:  $\{l_{b,1}, l_{b,2}, \dots, l_{b,L/2}\}$ . Let us consider the conditional probabilities  $P(l_{b,i}|l_{b,i-1})$ , i.e.: the probability of finding a bond-length  $l_{b,i}$  knowing that the previous bond-length was  $l_{b,i-1}$ . The independence assumption is equivalent to  $P(l_{b,i}|l_{b,i-1}) = P(l_b)$ , i.e.: that knowledge of the previous bond-length is irrelevant. In fact, this assumption is *false*. After a bond of length  $l_{b,i-1} = 3$ , a bond  $l_{b,i} = 1$  must ensue. Nonetheless, the difference  $|P(l_{b,i}|l_{b,i-1}) - P(l_b)|$  decays to zero very fast when  $l_{b,i-1}$  grows. Since the contribution to the entropy is larger for larger bonds, the independence assumption becomes accurate in that case.

### A. Order Statistics for the Bond-Length

Let  $\pi_k(l_b)$  denote the probability distribution function (PDF) for the  $k$ -th longest bond. Thus,  $\pi_1(l_b)$  will be the PDF for the longest bond in the system,  $l_{b,max}$ . Figure (12) shows the histogram found over five million realizations with  $\delta = 10$  for  $L = 32$  and  $L = 64$  with the RG. A thermodynamic limit curve appears for those relatively small sizes, with a peak at  $l_{b,max}/L \approx 0.2$ , i.e.: the longest bond covers approximately  $1/5$  of the total system. After the maximal bond, the curve appears almost flat, up to  $1/2$ , which is the maximal realizable value.

The independence assumption allows us to give an estimate for  $\pi_1(l_b)$ . Let  $X$  be a 1D random variable with probability distribution  $P(X)$ , and  $X_{max,N}$  represent the maximal observation out of a series of  $N$  independent realizations. The probability distribution for  $X_{max,N}$  can be found this way: (i) find the cumulative distribution function (CDF) for  $X$ :  $F(x) \equiv P(X > x) = \int_{-\infty}^x p(s) ds$ ; (ii) the CDF for the maximal observation is just  $P(X_{max,N} > x) = F(x)^N$ ; (iii) the probability distribution for the maximal observation is found by differentiation of the CDF:  $P(X_{max,N}) = \partial_x [F(x)^N]$ . Since

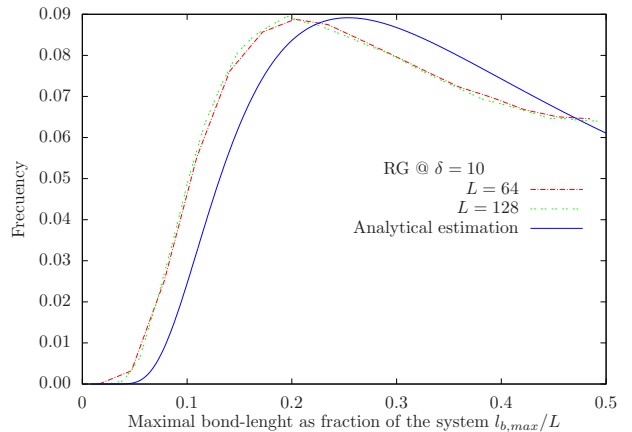


Figure 12: Histogram for  $l_{b,max}/L$  in the IRFP. Notice how both curves seem to converge to a thermodynamic limit. For low  $l_{b,max}$ , the probability increases fast up to a value  $l_{b,max}^M/L$ , which is close to 0.2. The continuous curve corresponds to the estimate for  $\pi_1(l_b)$  given in equation (20).

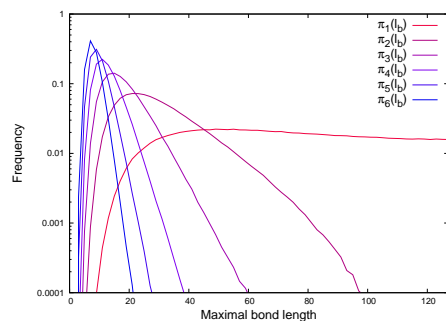


Figure 13: Probability distribution functions for the  $k$ -th longest bond in a chain with 256 sites, with  $\delta = 10$  and  $10^6$  realizations.

we have  $L/2$  bonds in our system, the CDF for the maximal bond will be  $F(l_b)^{L/2}$ . Assuming a continuous PDF  $P(l_b) \propto l_b^{-2}$ , we get the estimate

$$\pi_1(l_b) \propto \left(1 - \frac{1}{l_b}\right)^{L/2-1} \left(\frac{1}{l_b^2}\right). \quad (20)$$

This estimate, which is plotted in fig. (12), can be used to find the value of  $l_{b,max}^M$ , the most likely maximal bond-length. In the thermodynamic limit,  $l_{b,max}^M \approx L/4$ .

Figure (13) depicts the different  $\pi_k(l_b)$ , i.e.: the PDF for the  $k$ -th longest bond, for a system with 256 sites and  $10^6$  disorder realizations. Notice how they become more and more peaked as  $k$  increases.

### B. Longest bond and energy gap

The average energy gap  $\Delta E$  is known to vanish very fast in the thermodynamical limit [23]. In this section we will consider the relation between this average gap and entanglement. Since energy scales are linked to length



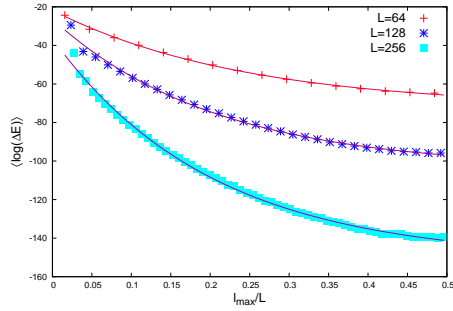


Figure 14: Average logarithm of the energy gap as a function of the  $l_{b,\max}$  in each realization, for three system sizes ( $L = 64, 128$  and  $256$ ), and  $\delta = 8$ . Alongside, fit to functional form (21).

scales, the connection is made via the longest bond. We have applied the Dasgupta-Ma RG to  $10^6$  disorder realizations with  $\delta = 8$  for systems of  $L = 64, 128$  and  $256$ . The average value of  $\log(\Delta E)$  for each value of  $l_{b,\max}$  fits to an exponential decay:

$$\langle \log(\Delta E) \rangle \approx A + B \exp(-l_{b,\max}/l_0) \quad (21)$$

In all three cases,  $l_0 \approx L/5$ , i.e.: the expected value for the maximal bond-length.

## V. RANDOM PERMUTATIONS AND ENTANGLEMENT

A simple model can be devised which reproduces most features of the ground state of the random hopping model, in which all the disorder effects are collected into a model of *random permutations*.

Let us consider a variant of the random hopping model in which each new disorder realization is associated with a random permutation  $\sigma$  of the set  $\{1, \dots, L\}$ . Let us associate the  $i$ -th element of the permutation,  $\sigma_i$ , to the  $i$ -th hopping term of the chain:  $J_i = \exp(-\sigma_i)$ . The rationale is that the renormalization rule eq. (8) becomes now additive in the values of  $\sigma_i$ :

$$\sigma_i^{(R)} = \sigma_{i+1} + \sigma_{i-1} - \sigma_i, \quad (22)$$

i.e.: the lowest element of the permutation is removed, along with its two neighbors, and all three are replaced by a renormalized element. Each random permutation determines a bond-structure, which in turn determines all the correlation and entanglement properties within the ground state of the system. Thus, we conjecture that sampling over disorder realizations amounts to sampling over random permutations, i.e.: a discrete set of possibilities. Random permutation theory has already made appearance in other areas of physics, such as the statistical mechanics of growing interfaces [24], where it links the shape fluctuations in the Kardar-Parisi-Zhang (KPZ) universality class with the Tracy-Widom probability distributions from random matrix theory.

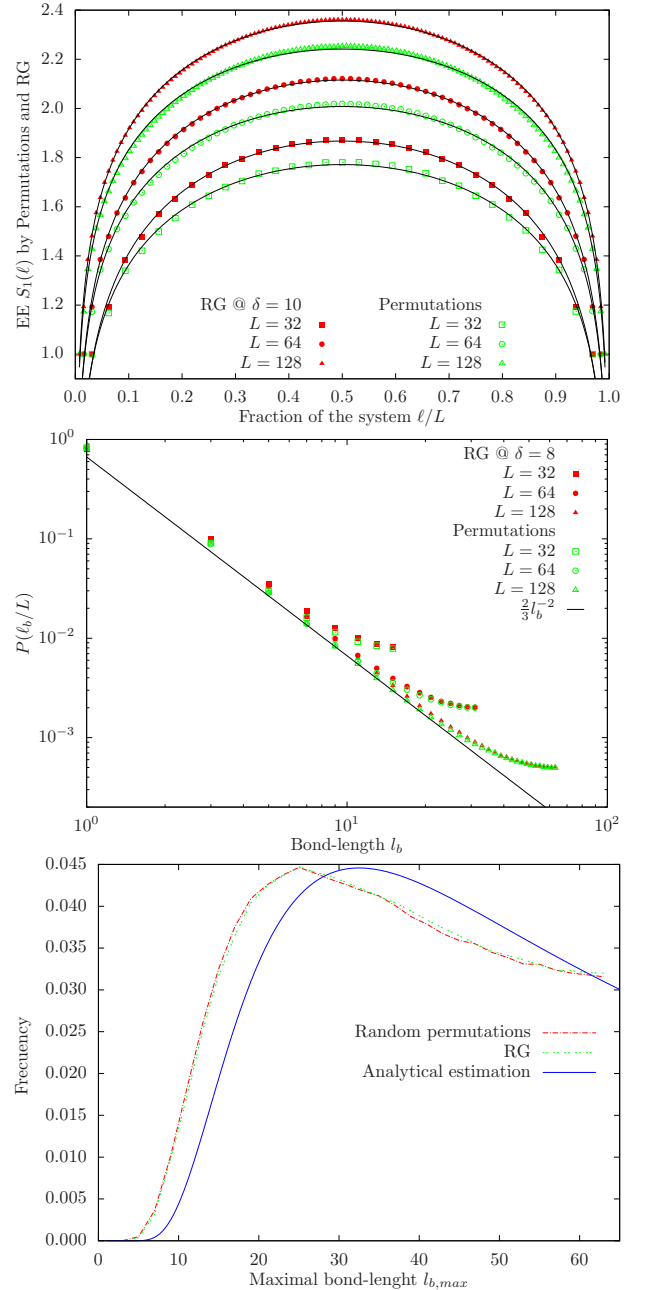


Figure 15: Study of entanglement of the ground state of the random permutations model. Top: average von Neumann entropy as a function of  $\ell/L$ , for  $L = 32, 64$  and  $128$ . Center: Histogram for the bond lengths,  $l_b$ . Bottom: Histogram for  $l_{b,\max}/L$  obtained by RG and random permutations for  $L = 128$ . Notice how both curves seem to converge to a thermodynamic limit. For low  $l_{b,\max}$ , the probability increases fast up to a value  $l_{b,\max}^M/L$ , which is close to 0.2.

Our RG flow in the permutation space is not perfectly determined. It sometimes finds *coincidences*, i.e.: despite all elements are initially different, after some RG steps, some of them will coincide. If the coinciding elements are sufficiently far apart, the order in which we renormalize them is immaterial. In a few cases, they are close enough,

thus forcing to choose one of them randomly in order to proceed. Nonetheless, those coincidences get more and more sparse as the system size grows, and become negligible in the thermodynamic limit.

Let us show that the Dasgupta-Ma RG and the random permutations model give the same results for the entanglement. As it was discussed above, all the relevant magnitudes stem from a single function: the probability distribution for  $P(l_b)$ . Figure (15) shows runs performed for  $10^5$  samples for  $L = 32, 64$  and  $128$  for the average von Neumann entropy (top), bond length histogram (center) and maximal bond length histogram (bottom), along with comparison with the Dasgupta-Ma RG approach.

$L$	Permutations			RG		
	$c$	$c'$	$\chi^2/10^{-4}$	$c$	$c'$	$\chi^2/10^{-4}$
32	1.043	0.567	2.2	1.167	0.519	2.3
64	1.047	0.557	1.4	1.148	0.524	1.0
128	1.048	0.547	1.2	1.124	0.538	0.5

Table I: Fitting values for the von Neumann entanglement entropy (see eq (9)) to compare the model of random permutations and the RG method for  $\delta = 10$  and  $5 \cdot 10^6$  samples.

The main feature of the random permutations model is the strong hierarchy among the link strengths. Our model bears strong similarities to the *hierarchical model* of RNA-folding [25, 26]. In this model, random binding energies are provided for each pair of sites on a 1D chain, and bonds are established among them in order with a no-crossing condition. Renormalization group arguments show that the universality class is captured merely by choosing the  $L(L-1)/2$  binding energies  $\epsilon_{ij}$  such that  $\epsilon_{i_1 j_1} \ll \epsilon_{i_2 j_2} \ll \dots \ll \epsilon_{i_{L(L-1)/2} j_{L(L-1)/2}}$ . This model can be considered an infinite-dimensional version of the random hopping model.

## VI. EXCITED STATES

Entanglement of excited states has been studied recently within the CFT framework [20, 27–31]. In this section we will extend the techniques developed in our work to study the excited states of the random hopping model. Indeed, entanglement of all eigenstates can be constructed using either exact diagonalization, Dasgupta-Ma RG or random permutations approaches. As it has been stated above, the eigenstates of the hopping matrix constitute the single-body modes: bonds between pairs of sites, with negative energy, and their corresponding anti-bonds, with positive energy. The ground state is obtained by filling up the set of all negative energy modes, i.e.: all the bonds. The full spectrum of the Hamiltonian is obtained as we either reduce the number of particles to allow empty modes and/or add particles in modes with positive energy. Both negative and positive energy modes, bonds and anti-bonds, give the same contribution to the entanglement entropy but, when both

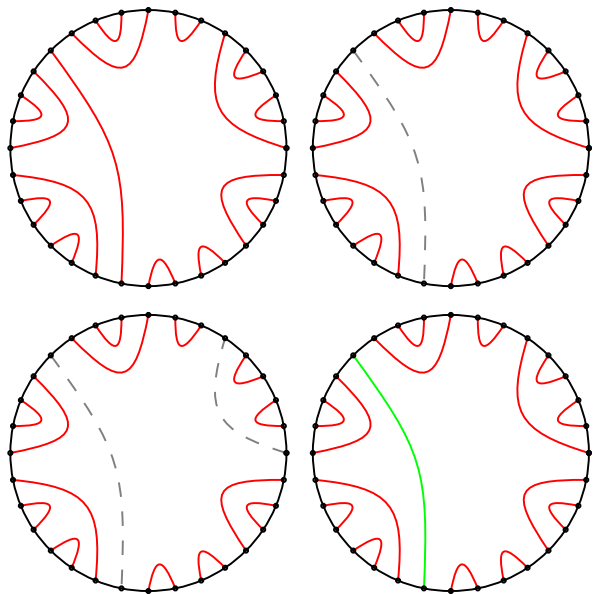


Figure 16: Pictorial representation of the excited states. Top-left: Bond-structure of the ground state  $|0\rangle$ . Top-right: the excited state  $|1\rangle$  is obtained by removing the longest bond. Bottom-left: if the second longest bond is removed, the excited state  $|2\rangle$  is obtained. Bottom-right: the PH state is built by upgrading the closest particle to the Fermi point to the first mode above it. Due to the particle-hole symmetry, in our case we upgrade the longest bond to the corresponding anti-bond, which presents the same entanglement.

are present on the same pair of sites, their contribution to entanglement cancels out, leaving two factorized sites.

For a clean system, the entanglement entropy increases substantially when a particle-hole (PH) excitation is created, i.e.: when a particle in an occupied mode is upgraded to an empty state above the Fermi level [28, 31]. Moreover, entanglement remains invariant for *compact states*, i.e.: states in which the list of occupied modes presents no holes. Those states are represented by vertex operators.

The situation is very different for the strongly disordered system. Figure (16) illustrates the different types of excited states and their effects on entanglement. In the top-left panel we show a possible bond structure describing the ground state. The lowest energy excitation is the compact state obtained by either removing the weakest bond or adding a particle on the weakest anti-bond. Both cases result in the longest bond being removed from the system, as shown in the top-right panel. A second compact excitation can be obtained by removing/adding a further particle, as shown in the bottom-left panel. The last panel shows the effect of a PH excitation, in which the longest bond is upgraded to be an anti-bond, which leaves the entanglement structure untouched.

Let  $|x\rangle$  denote the excited state in which  $x$  particles have been removed from the ground state (equivalently, we could say added), and let  $S(\ell, x)$  denote the average von Neumann entropy of a block of size  $\ell$  within state  $|x\rangle$ .

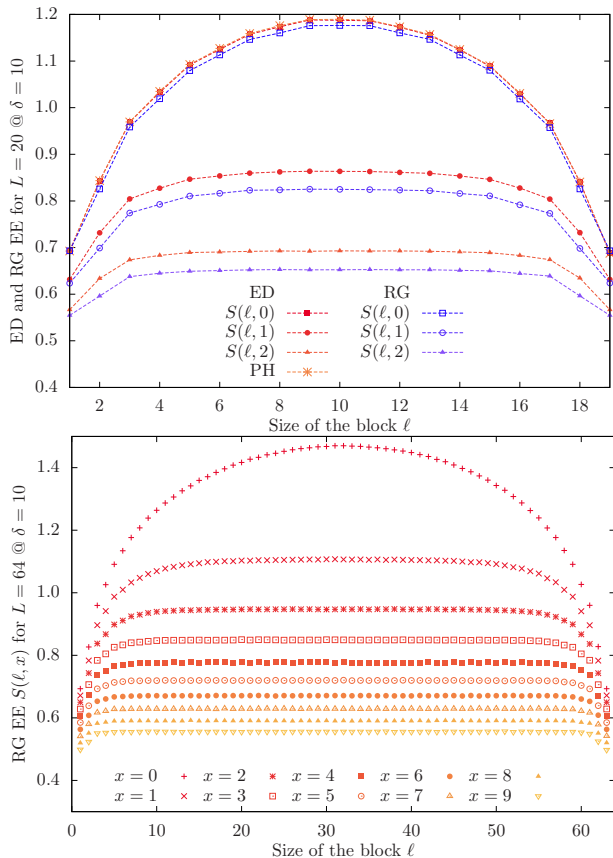


Figure 17: Top: Average von Neumann entropy of the ground state and low-energy excited states, both with exact diagonalization and RG. Note the decrease of the entropy in the case of excited states  $|1\rangle$  and  $|2\rangle$ , and the invariance for the PH excitation. Bottom:  $S(\ell, x)$  for a system of 64 sites for different number of removed/added particles  $x$  ( $x=0$  corresponds to the ground state).

Figure (17, top) shows this average von Neumann entropy for the ground state and three excited states, obtained with exact diagonalization and the RG. The first one, the PH excitation, coincides with the entanglement of the ground state. The other two correspond to states  $|1\rangle$  and  $|2\rangle$ , in which one ( $S(\ell,1)$ ) or two ( $S(\ell,2)$ ) particles are added or removed. Notice that, in this case, a *plateau* appears for intermediate block sizes, similar to the one appearing for the ground state of odd-sized systems. The bottom panel of fig. (17) shows how this plateau reduces slowly its height as the number of added/removed particles increases, i.e.: the curves  $S(\ell, x)$  flatten progressively for increasing  $x$ .

Figure (18, top) shows the behavior of  $S(\ell, 1)$  for sizes ranging from  $L=32$  to  $L=2048$ , as obtained with the RG. All of them present a similar plateau, but at increasing heights. Notice that the sizes are in geometric progression, and the plateau heights appear to grow only arithmetically. This shows that the behavior of  $S(L/2, 1)$  is *logarithmic* with the system size  $L$ . Indeed, let us claim that

$$S(L/2, x) = \frac{c_{ex} \log(2)}{3} \log(L) + c'_{ex}(x). \quad (23)$$

with  $c_{ex} = 1$ . This claim receives support from the results shown in the bottom panel of fig. (18), which shows  $S(L/2, x)$  as a function of  $L$  (in logarithmic scale), for different values of  $x$ . Notice that all curves are, in fact, parallel straight lines, and the slope is indeed close to  $\log(2)/3$ . The additive constant  $c'_{ex}(x)$  is the only difference, and its decay with  $x$  is shown in the inset of fig. (18). For the  $x=1$  case, the reduction in the value of the additive constant from the ground state can be explained by assuming a reduced *effective system size*, from  $L$  to  $L/5$ , i.e.:  $c'_{ex}(1) \approx c' - \log(2) \log(5)/3$ . This reduction in the effective system size can be explained if we assume that it coincides with the *length of the expected maximal bond*.

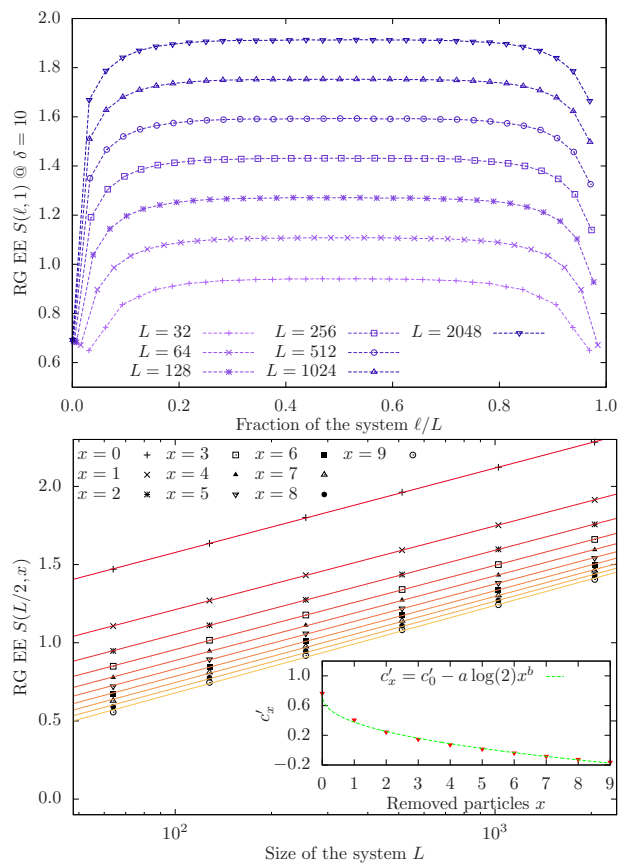


Figure 18: Top:  $S(\ell, 1)$  for different system sizes  $L = 32, 64, 128, 256, 512$  and  $1024$ . Notice that while the sizes grow geometrically, the maximal values of the entropy grow only arithmetically. Bottom: height of the *plateau* of  $S(L/2, x)$ , as a function of the system size, in solid lines represent the fit to expression (9), and the inset shows the additive constant  $c'_{ex}(x)$  as function of the removed particles ( $a = 0.56, b = 0.4$ ).

The curves  $S(\ell, 1)$  for different sizes collapse when the maximum value is subtracted from the entropy values

and, in the thermodynamic limit, they fit to the finite-size form:

$$S(\ell, 1) \approx \frac{c \log(2)}{3} \log(L) + c'_x - \beta e^{-\gamma \sqrt{\ell/L}} \quad (24)$$

where  $\gamma \approx 10$  allows us to estimate the size of the region in which entropy grows to reach the value  $S(L/2, 1)$  as approximately  $1/5$  of the total size of the system. Remarkably,  $L/5$  is again the average size of the bond of maximal length, as shown in figure (12).

From all those analysis we can attempt a physical picture of the entanglement in the first excitation. Removal of the weakest bond is usually the same as a removal of the longest bond, which has a typical size  $l_{b,max} \approx L/5$ . Since bonds can not cross, entanglement can grow normally only *within* the region of size  $\approx L/5$  which lies under this longest bond. The region outside, with size  $4L/5$ , is devoid of long bonds, and contributes less to the entanglement. Similar arguments apply for the higher excitations.

## VII. CONCLUSIONS

In this work we have analyzed the properties of entanglement in random hopping models, focusing on the similarities between the CFT predictions for the clean case and the strong disorder RG predictions. We have used a combination of exact diagonalization, the Dasgupta-Ma renormalization scheme and a new tool based on the study of random permutations. All techniques coincide in providing a compelling image, based on a bond-picture.

All the entanglement properties within the ground state stem from the probability distribution for the bond lengths  $P(l_b)$  and an assumption of approximate independence for large bond lengths. Both the thermodynamic limit and the finite-size form for the average von Neumann entropy can be deduced from the scaling analysis of that distribution function. The behavior of the Rényi entropies can not be established solely from the bond picture, since the Dasgupta-Ma RG prediction is that all orders will give the same result. Indeed, we have observed that the parity oscillations which appear in the clean case, according to the CFT prediction, attenuate as the disorder grows, making them similar for all values of the Rényi order.

Interesting results were obtained for odd chains, where a *plateau* appears in the average von Neumann entropy, for intermediate system sizes. Moreover, parity oscillations appear both in the average von Neumann entropy of chains with open boundary conditions and in the *variance* of the von Neumann entropy in all cases. They fit nicely an expression similar to the CFT prediction, but with different constants. Remarkably, the scaling of the maximal variance is again logarithmic, but with a different prefactor.

We have introduced the *random permutation picture*, which is a simplification of the Dasgupta-Ma renormalization in which the hoppings are given fixed values which differ broadly in order of magnitude, but are distributed at random among the lattice links. All the properties of entanglement and correlation in the ground state can be established solely in this picture.

Furthermore, we have analysed the average entanglement of excited states. Indeed, excited states are of two types: those which convert a negative energy mode into its corresponding positive energy mode do not alter the bond picture. But excitations which add or remove particles alter them in a remarkable way. Indeed, the average entanglement entropy of the first excitation presents a *plateau* at intermediate sizes, whose magnitude scales logarithmically with the size of the system *as if* the size of the system corresponds to the average size of the maximal bond. Higher excitations result in a further reduction of the effective size of the system.

There are still many open questions related to this system. First of all, a thorough analysis of entanglement for intermediate values of the disorder would clarify the decay and convergence of the parity oscillations in the Rényi entropies of all orders. Moreover, it would be interesting to study the system from a dynamical point of view, i.e.: the clean to disorder transition.

## Acknowledgments

We would like to acknowledge F. C. Alcaraz and J. A. Hoyos for very useful discussions, along with CNPq for the hospitality at The São Carlos Institute of Physics (Brazil). We also acknowledge financial support from the Spanish government from grant FIS2012-33642. J.R.-L. acknowledges support from grant FIS2012-38866-C05-1.

- 
- [1] P. W. Anderson, *Phys. Rev.* **109** 1492 (1958).
  - [2] X. Jia, A. R. Subramaniam, I. A. Gruzberg, and S. Chakravarty, *Phys. Rev. B* **77**, 014208 (2008).
  - [3] C. Holzhey, F. Larsen, and F. Wilczek, *Nucl. Phys. B* **424**, 443 (1994).
  - [4] G. Vidal, J. I. Latorre, E. Rico, and A. Kitaev, *Phys. Rev. Lett.* **90**, 227902 (2003).
  - [5] P. Calabrese and J. Cardy *J. Phys. A: Math. Theor.* **42**, 504005 (2009).
  - [6] G. Refael and J. E. Moore, *J. Phys. A: Math. Theor.* **42**, 504010 (2009).
  - [7] M. Fagotti, P. Calabrese, and J. E. Moore, *Phys. Rev. B* **83**, 045110 (2011).
  - [8] O. Boada, A. Celi, J. I. Latorre, and M. Lewenstein, *New J. Phys.* **13**, 035002 (2011).
  - [9] C. Dasgupta and S. K. Ma, *Phys. Rev. B* **22**, 1305 (1980).
  - [10] D. S. Fisher, *Phys. Rev. B* **51**, 6411 (1995).
  - [11] D. S. Fisher and A. Young, *Phys. Rev. B* **58**, 9131 (1998).

- [12] I. Peschel, *J. Phys. A: Math. Gen.* **36**, L205 (2003).
- [13] A. M. Goldsborough and R. A. Römer, *Self-assembling tensor networks and holography in disordered spin chains*, [arXiv:1401.4874](#) (2014).
- [14] N. Laflorencie, *Phys. Rev. B* **72**, 140408(R) (2005).
- [15] G. Refael and J. Moore, *Phys. Rev. Lett.* **93**, 260602 (2004).
- [16] P. Calabrese and J. Cardy, *JSTAT* P06002 (2004).
- [17] J. C. Xavier and F. C. Alcaraz, *Phys. Rev. B* **83**, 214425 (2011).
- [18] P. Calabrese, M. Campostrini, F. Essler, and B. Nienhuis, *Phys. Rev. Lett.* **104**, 095701 (2010).
- [19] H. F. Song, S. Rachel, and K. Le Hur, *Phys. Rev. B* **82**, 012405(2010).
- [20] L. Taddia, J. C. Xavier, F. C. Alcaraz, and G. Sierra, *Phys. Rev. B* **88**, 075112 (2013).
- [21] M. Dalmonte, E. Ercolessi, and L. Taddia, *Phys. Rev. B* **84**, 085110 (2011).
- [22] J. A. Hoyos, A. P. Vieira, N. Laflorencie, and E. Miranda, *Phys. Rev. B* **76**, 174425 (2007).
- [23] D. S. Fisher, *Phys. Rev. B* **50**, 3799 (1994).
- [24] T. Kriecherbauer and J. Krug, *J. Phys. A: Math. Theor.* **43**, 403001 (2010).
- [25] M. Müller, *Repliments d'hétéropolymères*, Ph.D. thesis, Univ. Paris XI Orsay (2003).
- [26] F. David, C. Hagendorf, and K. J. Wiese, *JSTAT* P04008 (2008).
- [27] F. C. Alcaraz, M. Ibáñez, and G. Sierra, *Phys. Rev. Lett.* **106**, 201601 (2010).
- [28] M. Ibáñez, F. C. Alcaraz, and G. Sierra, *JSTAT* P08025 (2012).
- [29] M. Dalmonte, E. Ercolessi, and L. Taddia, *Phys. Rev. B* **85**, 165112 (2012).
- [30] D. Eloy and J. C. Xavier, *Phys. Rev. B* **86**, 064421 (2012).
- [31] F. H. L. Essler, A. M. Läuchli, and P. Calabrese, *Phys. Rev. Lett.* **110**, 115701 (2013).
- [32] T. G. Rappoport, L. Ghivelder, J. C. Fernandes, R. B. Guimarães, and M. A. Continentino, *Phys. Rev. B* **75**, 054422 (2007).
- [33] P. G. de Gennes, *Biopolymers* **6**, 715 (1968).